UCLA
UCLA Previously Published Works

Title

Complementary radial tagging for improved myocardial tagging contrast

Permalink

Journal

ISSN

Authors

Wang, Zhe
Nasiraei-Moghaddam, Abbas
Reyhan, Meral L
et al.

Publication Date

DOI

Peer reviewed

Complementary Radial Tagging for Improved Myocardial Tagging Contrast

Zhe Wang,[1,2] Abbas Nasiraei-Moghaddam,[1,3] Meral L. Reyhan,[1,4] Subashini Srinivasan,[1,2] J. Paul Finn,[1,4] and Daniel B. Ennis[1,2,4]*

Purpose: To develop and evaluate complementary radial tagging (CRT) for improved myocardial tagging contrast.
Methods: We sought to develop and evaluate CRT, which aims to preserve the radial tag contrast throughout the cardiac cycle. Similar to complementary spatial modulation of magnetization, CRT acquires two sets of images with a phase shift in the tag pattern. The combination of a ramped imaging flip angle and image subtraction enhances tag contrast throughout the cardiac cycle. The proposed CRT technique uses a small table shift away from the isocenter to improve the uniformity of the radial tag pattern. We provide a mathematical solution for the optimal table shift and validate the solution in using a retrospective analysis of images from 500 patients in the Cardiac Atlas Project database.
Results: CRT simulations, phantom experiments, and in vivo images all demonstrate the improved tag contrast of CRT compared to RT. The retrospective evaluation demonstrated that acceptable CRT images could be acquired in over 98% of the clinical exams.
Conclusion: The CRT technique improves radial tag contrast throughout the cardiac cycle and should produce high quality tag patterns in nearly all patients. **Magn Reson Med 73:1432–1440, 2015. © 2014 Wiley Periodicals, Inc.**

Key words: myocardial tagging; complementary radial tagging; spatial modulation of magnetization; complementary spatial modulation of magnetization

INTRODUCTION

Cardiac magnetic resonance imaging is a proven technique for the evaluation of myocardial structure and function. In particular, MRI tagging can be used to noninvasively generate tissue landmarks, which facilitate the qualitative and quantitative assessment of left ventricular (LV) myocardial deformation in both research and clinical settings (1–3). The first demonstration of myocardial tagging by Zerhouni et al. (1) used radial saturation bands. Therein, several thin tagging planes were generated perpendicularly to the imaging plane. During imaging, the tagging planes appear as dark lines within the imaging plane and the tag pattern deformation reflects the underlying myocardial motion. This method of tag generation was surpassed by Cartesian line or grid tagging patterns, which can be generated by spatial modulation of magnetization (SPAMM) (2). T_1 relaxation effects, however, contribute to tag fading, which typically result in the tags only being detectable for the first ∼500 ms of the cardiac cycle at 1.5 T (4). Complementary spatial modulation of magnetization (CSPAMM) was introduced by Fischer et al. (5) to enhance tag contrast and increase the tag persistence in late cardiac phases.

Recently, Nasiraei-Moghaddam and Finn (6) developed a new pulse sequence, which uses time-varying sinusoidal-shaped RF pulse and gradients to generate radial tags efficiently. Whereas previous radial tagging techniques used multiple discrete RF pulses within a relatively long tag preparation time, this radial tagging sequence uses continuous RF pulses and gradient waveforms. Due to the contribution of both on-resonance excitation and off-resonance excitation, this radial tagging method has lower specific absorption rate and can be generated in a shorter period of time compared to previous radial tagging sequences.

Radial tagging patterns have the potential advantage of better conforming to the annular geometry of the LV in the short axis (SA) view, but no radial tagging technique has been presented that produces contrast similar to CSPAMM. Hence, in this article, we define the principles that govern combining the CSPAMM concept with radial tag encoding to create complementary radial tags (CRT); demonstrate LV SA images acquired in healthy subjects; and discuss the requirements for obtaining high quality CRT images. The in vivo tag contrast is also compared with theoretical simulation results. Furthermore, with the CRT technique used herein the scanner table is translated to an optimal table position relative to the isocenter of the main magnetic field to improve the uniformity of the radial tag pattern. Lastly, we use the Cardiac Atlas Project (7) to retrospectively calculate the optimal table position of LV SA images from a large population of patients and demonstrate that the new CRT technique can be used in the majority of clinical cases.

THEORY

Complementary Radial Tagging

We combine the principle of CSPAMM (5) with the radial tag encoding technique (6) to generate CRT

[1]Department of Radiological Sciences, University of California, Los Angeles, California, USA.

[2]Department of Bioengineering, University of California, Los Angeles, California, USA.

[3]Department of Biomedical Engineering, Amirkabir University of Technology, Tehran, Iran.

[4]Biomedical Physics Interdepartmental Program, University of California, Los Angeles, California, USA.

*Correspondence to: Daniel B. Ennis, Ph.D., Peter V. Ueberroth Building, Suite 1471, Room B 10945 Le Conte Avenue, Los Angeles, CA 90095. E-mail: daniel.ennis@ucla.edu
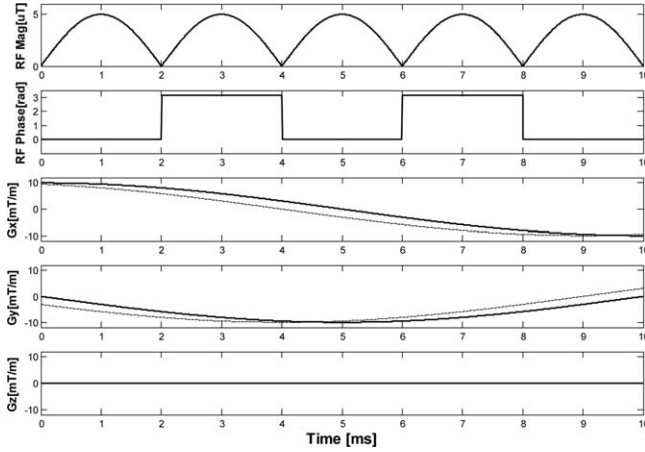
FIG. 1. RF pulse (magnitude and phase) and gradient waveforms for the CRT pulse sequence. Sinusoidal-shaped gradients generate one set of radial tags (solid line), while phase-shifted G_x and G_y gradients (dashed line) generate the complementary set of radial tags. The five sinusoidal lobes in the RF pulse create five radial tagging lines and 10 radial tags intersections with the LV wall. The number of tag intersections doubles again after CRT image subtraction.

images. Two series of RT images are encoded to generate phase-shifted tag patterns followed by a spoiled gradient imaging sequence. The pixel intensity in a RT image can be expressed by the sum of the image contrast profile (I_{image}) and the tag contrast profile (I_{tag}) (5).The tag profile is more easily expressed in polar coordinate system with the tag center as the origin, r as radius, θ as the polar angle, and t as time

$$I_{\text{total}}(r, \theta, t) = I_{\text{image}}(r, \theta, t) + I_{\text{tag}}(r, \theta, t) \qquad [1]$$

Two RT image sets have the same I_{image} ($I_{\text{image},1} = I_{\text{image},2}$). The subtraction of two RT image sets generates CRT images that contain only tag information.

$$I_{\text{total},1}(r, \theta, t) - I_{\text{total},2}(r, \theta, t) = I_{\text{tag},1}(r, \theta, t) - I_{\text{tag},2}\ (r, \theta, t) \qquad [2]$$

Two series of images are acquired with the same RF pulse, but sinusoidal gradients with different phases. The requisite phase shift (φ) between the gradients is:

$$\varphi = \frac{\pi}{2N_{\text{tag}}} \qquad [3]$$

N_{tag} is the number of tag lines. Consequently, the two tag profiles exhibit similar, but rotated tag patterns:

$$I_{\text{tag},1}(r, \theta, t) = I_{\text{tag},2}(r, \theta + \varphi, t) \approx -I_{\text{tag},2}(r, \theta, t) \qquad [4]$$

The two tag profiles have opposite signs and the tag contrast is, therefore, enhanced after subtraction.

$$I_{\text{total},1}(r, \theta, t) - I_{\text{total},2}(r, \theta, t) \approx 2\ I_{\text{tag},2}(r, \theta, t) \qquad [5]$$

Due to T_1 relaxation tag contrast gradually decreases and eventually becomes 0. Further application of the ramped imaging flip angle scheme on CSPAMM (5) images generate constant tag contrast throughout the

entire cardiac cycle. In this article, the ramped imaging flip angle scheme was used for image acquisition.

We use five half-sinusoid lobes for the RF pulse to generate a total of 10 intersections with the LV and 20 CRT line intersections after subtraction (Fig. 1). RF pulse not only excites the spins in the on-resonance plane to form a radial tag line but also contributes to circumferential adjacent lines, which sharpens the tag profile and leads to lower specific absorption rate of the preparation sequence compared to Zerhouni's methods. Also, note that the CRT approach requires fewer lobes compared to Nasiraei-Moghaddam's method to achieve the same number of tags.

Optimal Table Position

RT technique uses a combination of sinusoidal gradients and RF pulse envelopes to select an on-resonance plane, which rotates about the applied gradient direction ($\boldsymbol{g}$, unit vector, Fig. 2). The hardware design for modern MRI machines requires $\boldsymbol{g}$ pass through the isocenter (O) of the main (B_0) magnetic field. The intersection of $\boldsymbol{g}$ on the imaging plane defines the location of the radial tag center (C_{tag}). In general, the imaging plane can be described by a normal vector ($\boldsymbol{n}$, unit vector), which can be selected independent of $\boldsymbol{g}$.

Once a subject is positioned inside the MR scanner, the LV short axis plane's normal vector ($\boldsymbol{n}$) is defined relative to the scanner's coordinate system. If the angle (α) between $\boldsymbol{n}$ and $\boldsymbol{g}$ is minimized, then the intended radial tag pattern is generated, but the center of the radial tagging pattern is not guaranteed to coincide with the LV cavity center (C_{LV}; Fig. 2a). If, however, $\boldsymbol{g}$ is chosen to point to C_{LV}, but is not coaxial with $\boldsymbol{n}$, then α is not be minimized. Consequently, tagging will be centered correctly ($C_{\text{tag}} = C_{\text{LV}}$), but with nonuniform profile (Fig. 2b). The ideal radial tagging pattern is only generated when both $\boldsymbol{g}$ and $\boldsymbol{n}$ pass through C_{LV}, which requires: (1) $\boldsymbol{g}$ and $\boldsymbol{n}$ point to $C_{\text{LV}} = C_{\text{tag}}$. (2) Minimizing the angle (α) between $\boldsymbol{n}$ and $\boldsymbol{g}$ (Fig. 2b).

To satisfy requirement (1), C_{tag} is forced to coincide with C_{LV} by tilting the $\boldsymbol{g}$ away from the image plane normal $\boldsymbol{n}$ (Fig. 2b) such that $\boldsymbol{g} = M_{\text{rot}} \cdot \boldsymbol{n}$ where M_{rot} is a rotation matrix determined by the imaging plane parameters. This generates a projection of the radial tag pattern on the SA imaging plane (Fig. 2b).

To satisfy requirement (2), the scanner table can be moved away from the isocenter to an optimal table position (H_{opt}) to improve the tag profile. As indicated in Figure 2c, at the new table position, a uniform tag pattern is generated on a new oblique plane with a smaller α.

The ideal tag profile can be achieved when $\alpha = 0°$, however, the MRI scanner table can only be moved along the head-foot direction ($\pm H$ direction). In practice, for an arbitrary imaging plane in 3D space, α may only be reduced to a minimum, non-zero value.

$$H_{\text{opt}} = \text{argmin} < \alpha > \qquad [6]$$

The angle α between $\boldsymbol{g}$ and $\boldsymbol{n}$ and can be expressed as:

$$\alpha = a\text{cos}(\boldsymbol{g} \cdot \boldsymbol{n}) \qquad [7]$$
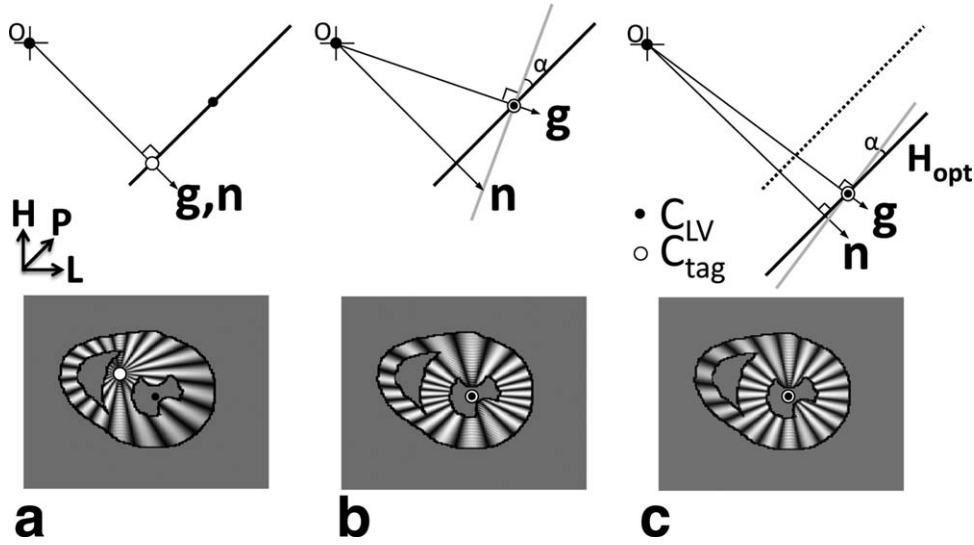
FIG. 2. Optimization of the position of the LV SA imaging plane (thick black line) and orientation of the tagging plane relative to the B_0 isocenter (O) to achieve the uniform radial tag pattern for the LV short axis. **a:** Subsequent to landmarking the gradient direction (**g**) used for tagging and the SA image plane normal (**n**) coincide, in general, but the center of the tags (C_{tag}) may not be coincident with the center of the LV (C_{LV}). **b: g** is updated to pass through the center of the LV (C_{LV} coincides with C_{tag}) and the tagging pattern is uniform on the tagging plane (gray line), but not on the SA imaging plane. **c:** Calculation of an optimal table shift ($H = H_{Opt}$) is achieved by minimizing α, which results in **g** intersecting C_{LV} and the optimum tagging pattern is generated on the SA imaging plane.

Once the imaging slice is defined, the image normal **n** is known:

$$\boldsymbol{n} = \begin{bmatrix} n_1 \\ n_2 \\ n_3 \end{bmatrix} \qquad [8]$$

g can be derived if C_{tag} is equivalent to C_{LV}

$$\boldsymbol{g} = \frac{1}{\sqrt{L^2 + P^2 + H^2}} \begin{bmatrix} L \\ P \\ H \end{bmatrix} \qquad [9]$$

L (left-right), P (anterior-posterior), and H (head-foot) indicate the subject's C_{LV} relative to isocenter (O). Substitution of Eqs. 8 and 9 into Eq. 7 results in the following:

$$\alpha = a \cos \left(\frac{n_1 L + n_2 P + n_3 H}{\sqrt{L^2 + P^2 + H^2}} \right) \qquad [10]$$

n_1, n_2, n_3, L, and P are fixed, whereas H remains the only variable. Take the derivative of Eq. 10 and set it to zero. H_{opt} can be derived as:

$$H_{opt} = \operatorname{argmin} \; <\alpha> = \frac{n_3(L^2 + P^2)}{n_1 L + n_2 P} \qquad [11]$$

METHODS

Complementary Radial Tagging Bloch Simulations

Radial tagging involves a highly nonlinear excitation of spins, wherein the pulse duration t, maximum RF amplitude $B_{1,max}$, maximum gradient amplitude G_{max}, and N_{tag}

contribute together to generate the radial tagging pattern (6). To better visualize and analyze the tagging pattern, simulated results were generated with a Bloch equation simulator (http://mrsrl.stanford.edu/~brian/bloch/) using MATLAB (The MathWorks, Natick, MA).

LV CRT images in the SA plane were simulated with the $T_1 = 1000$ ms (8), $T_2 = 60$ ms (8,9) representing myocardium at 1.5 T. The magnetization of the myocardium at thermodynamic equilibrium was set to one. Based on the average size of a normal human heart (10), an annulus of myocardium in the SA plane was defined with an inner diameter of 3 cm and an outer diameter of 5 cm. The following parameters were also used: 350×350 mm^2 field of view, 1.8×1.8 mm^2 pixel spatial resolution, $B_{1,max} = 5$ μT, $G_{max} = 10$ mT/m, and total tag preparation duration of 10 ms. The results were used to evaluate the tag pattern seen in Figure 2. Tag contrast ratio in RT and CRT simulations were calculated and compared with in vivo data in Figure 3.

Phantom Imaging Experiments

A stationary phantom was imaged using a 1.5 T Siemens Avanto scanner (Siemens Medical Solutions, Erlangen, Germany). The phantom's T_1 value was measured to be ~970 ms using spin echo inversion recovery. Similar to the traditional line or grid tag acquisitions, the CRT preparation module is played at the beginning of each cardiac cycle followed by spoiled gradient imaging acquisition. This modified spoiled gradient sequence with electrocardiogram (ECG) triggering was used to acquire images with different α for comparison to the simulation result. Imaging parameters were: total tagging preparation duration $= 10$ ms, TE/TR $= 3.75/5.13$ ms, field of view $= 250 \times 250$ mm^2, receiver bandwidth $= 200$ Hz/pixel, matrix size $= 196 \times 196$, and 1.3×1.3 mm^2
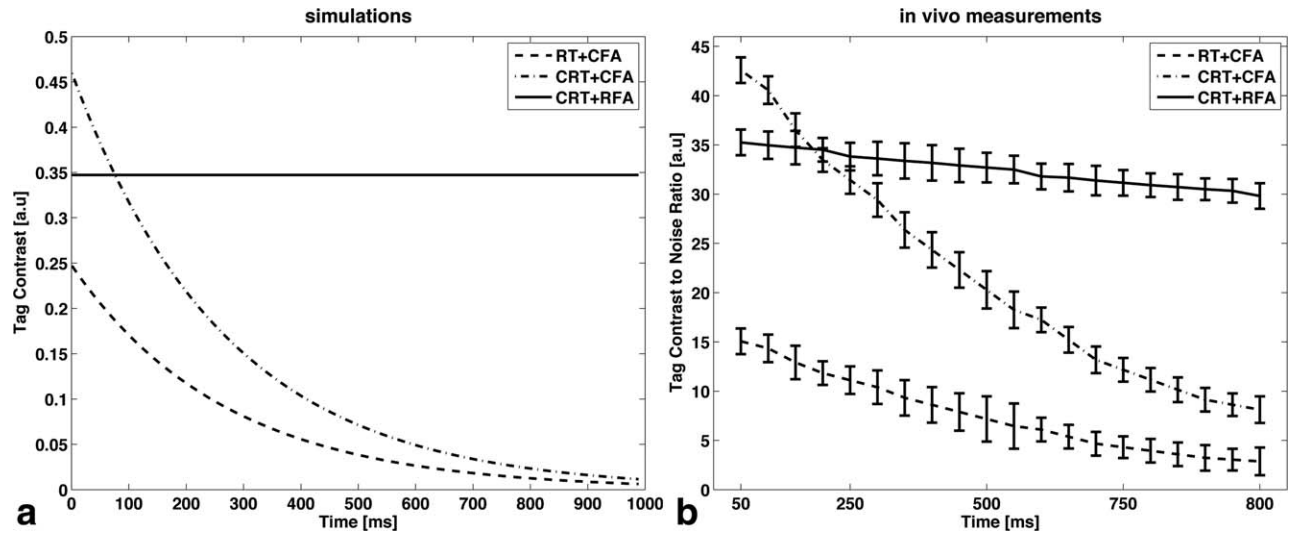
FIG. 3. **a:** Tag contrast in RT+CFA (dashed), CRT+CFA (dash dotted) and CRT+RFA (solid) images was calculated from simulation data. **b:** Tag contrast-to-noise ratio was measured in RT+CFA (dashed), CRF+CFA (dash dotted) and CRT+RFA (solid) in vivo images from 10 healthy volunteers. Error bars reflect the standard deviation for each cardiac phase.

resolution with slice thickness = 6 mm. External ECG trigger with RR interval of 1000 ms. Image flip angle is set to be 12°.

In the first experiment, tag pattern was generated on an oblique plane with different projection angle α. In the second experiment, C_{tag} was moved away from the C_{LV} with different off-center shift L to test the sensitivity of the correct placement of C_{tag} relative to C_{LV}. In both experiments, the arc length (d) between two adjacent tag lines was calculated and reported as mean ± standard deviation. The coefficient of variation (CV) is calculated as the standard deviation of d (d_{std}) divided by the mean of d (d_{mean}).

In Vivo Imaging Experiments

In accordance with institutional, state, and federal guidelines, all subjects were informed about the potential risks and benefits of the study and asked to provide signed statements of informed consent prior to commencing the imaging studies. The local institutional review board approved this study.

The CRT sequence used in the phantom experiment was slightly modified to acquire in vivo images. The new sequence included automated table position adjustments based on Eq. 11. In vivo images were acquired to demonstrate the CRT pattern in healthy volunteers ($N = 10$, 2 females and 8 males; age 26.5 ± 2.4 years) with no previous history of cardiovascular disease. Volunteers were positioned headfirst and supine. Localizer sequences and functional cine images were first acquired to locate the apical, middle, and basal slices in the cardiac SA plane using a six-element anterior coil array and a six-element posterior coil array. Short axis basal LV images were acquired at a basal position where the myocardium retains an annular shape for the entire cardiac cycle. Short axis apical LV images were acquired at the most apical level wherein the blood pool was apparent for all cardiac phases.

The following imaging parameters were used: total tag preparation duration was 10 ms, TE/TR = 3.75/5.13 ms, field of view = 300–350 × 300–350 mm², receiver bandwidth = 200 Hz/pixel, matrix size = 196 × 196, and 1.5–1.8 × 1.5–1.8 mm² resolution with slice thickness = 6 mm. Twenty cardiac phases were acquired using 8 k_y-lines per segment for a temporal resolution of 41 ms. A 12° constant imaging flip angle was used for the RT sequences to calculate the tag CNR and compared with tag contrast in simulation data. A ramped image flip angle with a final flip angle of 20° (11) was used for the CRT sequence to demonstrate the rather uniformed tag contrast throughout the entire cardiac cycle. The acquisition window was adjusted to cover ~90% of the R-R interval for each volunteer. Parallel imaging with rate-2 GRAPPA (12) and three-fourth partial Fourier imaging were used to reduce the total breath hold time to be 11–13 and 22–26 s for the RT and CRT sequences, respectively.

Both the phantom and in vivo CRT images were reconstructed offline using MATLAB. The CRT images were reconstructed by taking the complex difference of the two RT images for each cardiac phase.

Basal and apical LV SA tagged images were acquired from 10 healthy volunteers with off resonance insensitive SPAMM line tags (13) and CRT tags. LV twist from line and CRT tagged images was calculated using Fourier analysis of stimulated echoes (14). LV twist was calculated as the rotational difference between apical and basal LV images (15) for each cardiac phase.

Tag Contrast-to-Noise Ratio Measurement

The tag contrast-to-noise ratio (T_{CNR}) for RT and CRT in vivo images were measured in a subset of five healthy volunteers. Small regions-of-interests were placed on the tagged and untagged myocardium. The ratio of T_{CNR} between RT and CRT images was calculated and compared to the tag contrast (T_C) ratio acquired from noise-free simulation results. T_C and T_{CNR} are defined (16):
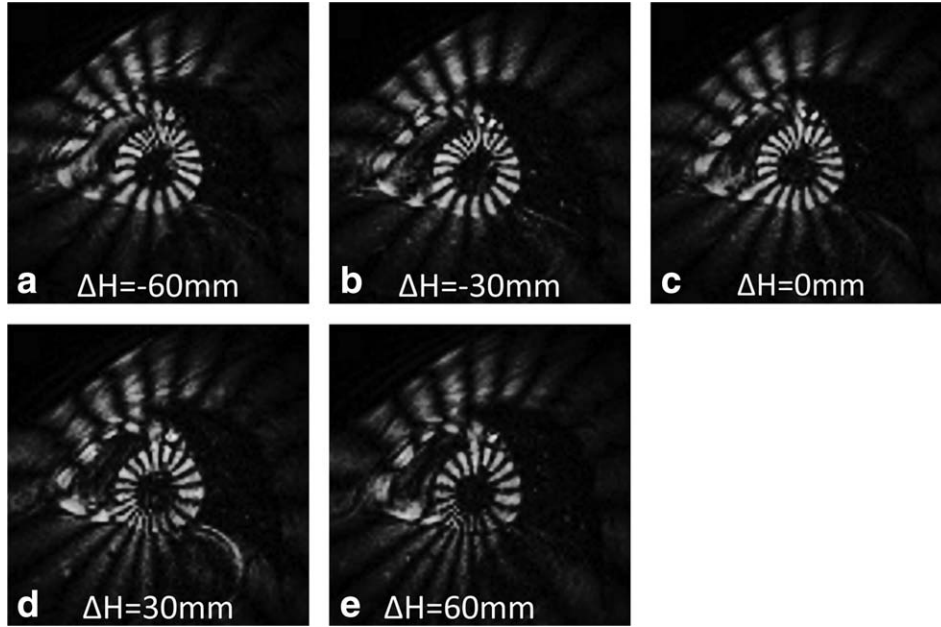
FIG. 4. CRT images acquired with a range of nonoptimal table position shifts. ΔH (mm) is defined as the table shift away from the optimal position. Note the tag pattern improvement in C where $\Delta H = 0$ mm and $H = H_{\text{opt}}$.

$$T_{\text{C}} = (\text{SI}_{\text{myocardium}} - \text{SI}_{\text{tag}}) \qquad [12]$$

$$T_{\text{CNR}} = \frac{(\text{SI}_{\text{myocardium}} - \text{SI}_{\text{tag}})}{\sigma_{\text{c}}} \qquad [13]$$

where $\text{SI}_{\text{myocardium}}$ and SI_{tag} are the mean regions-of-interest signal intensities for the untagged and tagged myocardial tissue and σ_{c} is the noise standard deviation (SD) measured from the background regions-of-interest and corrected by Dietrich et al.'s method (17).

Retrospective Analysis of Optimal Table Position Shifts

Though the hardware design varies among different MRI manufactures, the scanner table for modern MRI machines can only be moved within a limited range while maintaining image quality because of both the field homogeneity and the limits of gradient linearity. A previous study indicated images acquired out of this range (± 100 mm) suffer from severe gradient nonlinear distortion and the image quality can be affected dramatically (18). However, whether the optimal table position for a particular SA imaging slice falls within the gradient linearity range for most patients is unknown. Therefore, to evaluate the ability to acquire acceptable radially tagged images in clinical practice, the optimal table position shifts for a large number of subjects was retrospectively evaluated using images from the Cardiac Atlas Project database (7).

We retrospectively evaluated the H_{opt} and α values for 500 patients and 1537 LV SA images obtained from the Cardiac Atlas Project database. Patient-specific image information was extracted from the DICOM header file of each image including the normal of the image plane ($\boldsymbol{n}$), the pixel spacing value (pixel/mm), and the top-left pixel location (L, P, H). C_{LV} was manually identified for each image and transformed to scanner coordinates using information in the DICOM header. The image normal vector ($\boldsymbol{n}$) was obtained from the cross product of the two unit vectors along the image edge directions. The optimal table position and corresponding α_{min} for each patient and each SA plane was then calculated according to Eq. 11.

RESULTS

T_{C} and T_{CNR} Results

Figure 3a shows the tag contrast (T_{C}) as a function of time for RT with Constant Flip Angle (CFA), CRT with CFA, and CRT with ramped flip angles (RFA) from simulations. Figure 3b shows the mean T_{CNR} measured from in vivo images ($N = 10$). The simulation results show that the CRT+RFA maintains a constant T_{c} throughout the cardiac cycle. For the in vivo CRT measurements, subtraction of two image sets reduced the noise SD and further increased the T_{CNR} by a factor of about $\sqrt{2}$ compared to the RT sequence.

In Vivo Images

Figure 4 shows the CRT images at different table positions acquired in a healthy subject at $\sim$40% of the cardiac cycle. Figure 4a shows the nonuniform CRT pattern acquired 60 mm away from the optimal table position. The tag pattern improves as the table position approaches H_{opt} ($\Delta H = 0$) (Fig. 4b). The best CRT pattern is achieved when imaging at H_{opt} (Fig. 4c) and degrades beyond H_{opt} (Fig. 4d,e).

Figure 5 shows a comparison of the RT and CRT tag contrast different cardiac phases. LV SA images were acquired at the apical and basal levels. The dense tagging pattern combined with flowing blood results in the loss of tag information inside the LV cavity during all cardiac phases for both techniques. Additional blood pool suppression in the CRT images results from image subtraction. CRT technique combined with ramped imaging flip angle is used to obtain rather
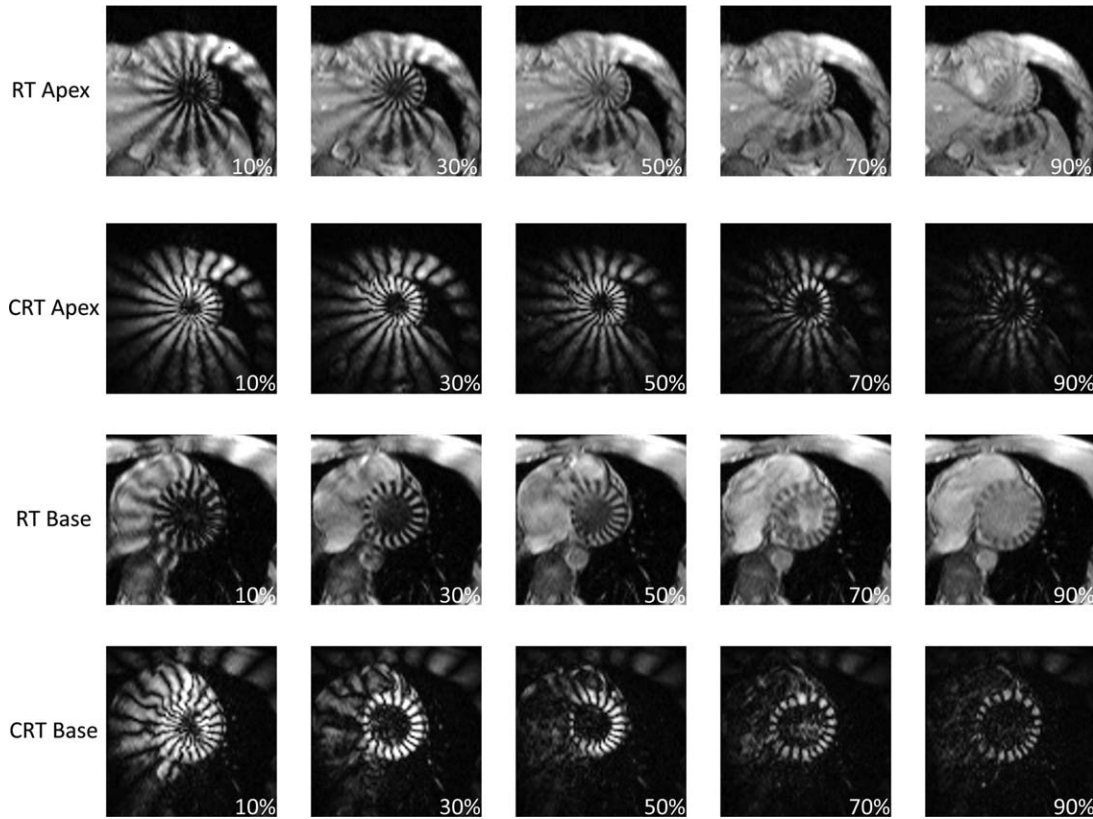
FIG. 5. Comparison between RT images and CRT images in a healthy human subject. For RT and CRT images, apical and basal LV images in the SA view are annotated as RT Apex, CRT Apex, RT Base, and CRT Base. The tag lines fade in RT images, but retain higher contrast in the CRT images, especially in the later cardiac phases.

uniform tag contrast throughout the entire cardiac cycle. The tags in the radial tagging images start to fade and become more difficult to observe in late cardiac phases, while the tag contrast is relatively preserved in the CRT images. Note also that due to tag fading in tissues outside the heart, there is significant background tissue suppression in CRT, which aids visualization of cardiac function.

Phantom Analysis

Equation 11 shows in some cases, α can be only minimized to a non-zero value. However, if α_{min} remains very large the tag profile is still significantly affected. The CRT profiles acquired in a stationary phantom with different projection angles are shown in Figure 6a. The white circle indicates the approximate LV
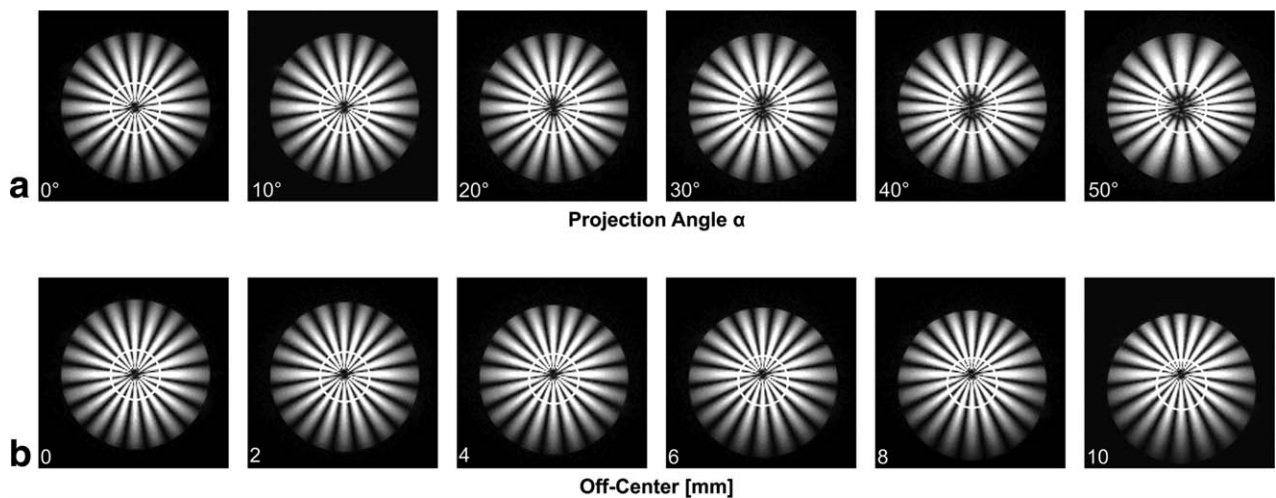

FIG. 6. **a**: CRT images with different projection angles α (0°, 10°, 20°, 30°, 40°, and 50°) were acquired in a stationary phantom. **b**: CRT images with the tag center moved away from the LV cavity by a distance L (0, 2, 4, 6, 8, and 10 mm). The white circle indicates the approximate myocardium location in LV SA image.

Table 1

Measured Distance between Adjacent Radial Tag Lines for a Range of Projection Angles (α) and Off-Center Distances (L) of the Radial Tags' Center (CV: Coefficient of Variation)

	Projection angle					
α (°)	0	10	20	30	40	50
d (mm)	6.7 ± 0.1	6.7 ± 0.3	6.7 ± 0.6	6.8 ± 1.3	6.8 ± 2.0	6.8 ± 2.8
CV	1%	4%	9%	20%	30%	41%
Off-center distance						
L (mm)	0	2	4	6	8	10
d (mm)	6.7 ± 0.1	6.7 ± 0.5	6.7 ± 0.9	6.7 ± 1.4	6.7 ± 1.8	6.7 ± 2.3
CV	1.5%	4.5%	9.0%	20%	27%	34%

myocardial position in a SA image. Results are reported in Table 1.

The in-plane image resolution for CRT in vivo images was $1.5–1.8 \times 1.5–1.8$ mm^2. Images with $\alpha \leq 30°$ have excellent tag profiles that are only subtly different from the ideal uniform tag profile (CV $\leq 20\%$, $d_{std} < 1$ pixel). For $30° < \alpha \leq 40°$ the tag profiles are affected, but still qualitatively acceptable (CV $\leq 30\%$, $d_{std} \approx 1$ pixel). When $\alpha > 40°$, a distinguishable pattern of more closely and more distantly spaced tags is apparent (CV $> 30\%$, $d_{std} > 1$ pixel). Based on these images, we conclude that $\alpha \leq 30°$ produces an excellent tag pattern, whereas $\alpha \leq 40°$ produces an acceptable tag pattern, but $\alpha > 40°$ produces an unacceptable tag pattern.

In Figure 6b, C_{tag} was moved away from C_{LV} with different off-center shifts L, d is calculated for each L in Table 1. When the C_{tag} does not coincide with C_{LV} we find that d_{std} 1.4 (<1 pixel) and the CV $\leq 20\%$ if $L < 6$ mm and that the tag pattern is more variable for $L > 6$ mm.

Retrospective Analysis

Figure 7 shows a two-dimensional histogram from the retrospective analysis of patients ($N = 500$) in the Cardiac Atlas Project database. The x-axis shows the absolute value of the optimal table position($|H_{opt}|$) and the y-axis shows the corresponding minimum projection angle (α_{min}). Analysis of the 2D histogram demonstrates that 90% (1383/1537) of the clinical cases fall within $\alpha_{min} \leq 30°$ and $|H_{opt}| \leq 55$ mm (Fig. 7 solid white line), which should produce an excellent CRT pattern. An acceptable tag pattern can be generated in 99% (1521 of 1537) of the clinical cases (Fig. 7 dashed white line) when $\alpha_{min} \leq 40°$ and $|H_{opt}| \leq 70$ mm).

LV Twist Analysis

Figure 8 demonstrates the LV twist measurement using the Fourier analysis of stimulated echoes method for off resonance insensitive SPAMM line tagged and CRT tagged images in 10 healthy volunteers. t-test between the two measurement results show no statistical differences ($P = 0.28$). Linear regression results in a correlation
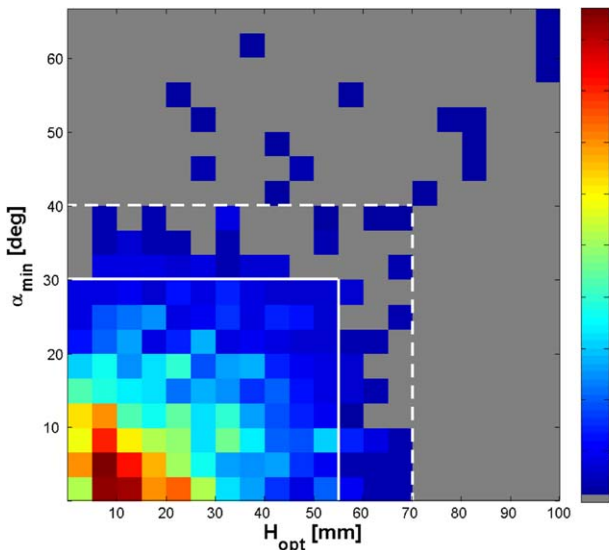

FIG. 7. Two-dimensional histogram of the optimal table position shift ($|H_{opt}|$) and minimum projection angle (α_{min}) for 1537 SA images retrospectively analyzed from patients ($N = 500$) in the Cardiac Atlas Project database. A cut-off of $|H_{opt}|$ is applied. $\alpha_{min} \leq 30°$ and $|H_{opt}| \leq 55$ mm (solid white line) indicates 90% clinical cases could have been imaged with an excellent radial tagging profile. $\alpha_{min} \leq 40°$ and $|H_{opt}| \leq 70$ mm (dashed white line) indicates 99% clinical cases would have an acceptable radial tagging profile.
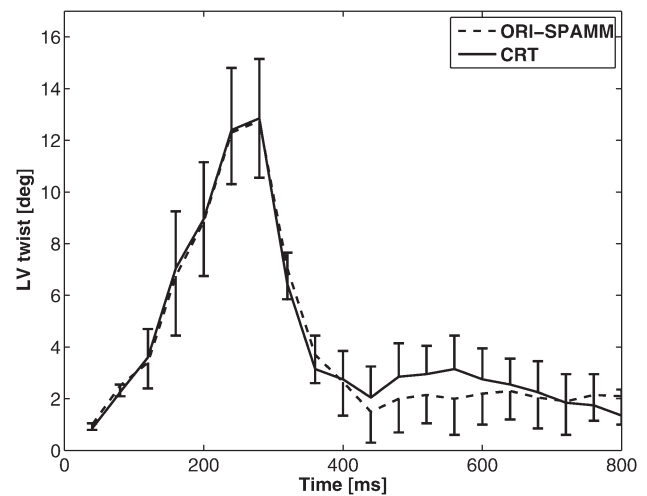

FIG. 8. LV mean twist measurement from 10 healthy volunteers using Fourier analysis of stimulated echoes method for CRT (solid) and off resonance insensitive SPAMM line tagged images (dashed). The one-sided error bars reflect the standard deviation for each cardiac phase.
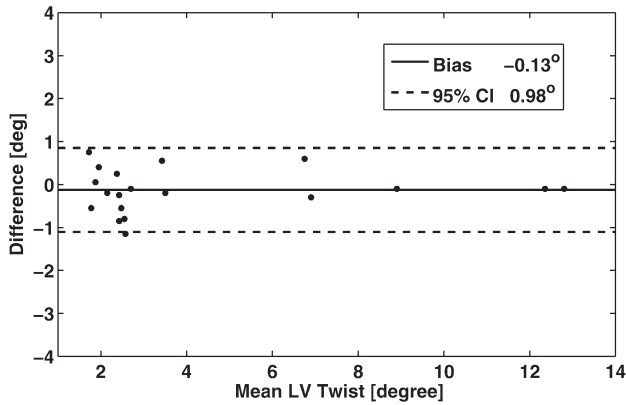
FIG. 9. Bland–Altman plot comparing the LV twist measurements obtained using the off resonance insensitive SPAMM and CRT methods.

coefficient of $r = 0.99$. Figure 9 shows the Bland–Altman analysis with a measured bias of $-0.13°$ and a 95% confidence interval of $\pm 0.98°$. There are small apparent differences in mid-diastasis and late diastolic phases between the two tagging methods compared with the subtle apparent differences during systole.

DISCUSSION

In this article, we defined the theory, demonstrated simulation and phantom results, and evaluated in vivo images using CRTs. CRT extends tag contrast throughout the cardiac cycle and affords the potential advantages of a tagging pattern that is more closely matched to the annular geometry of the LV.

Simulation results show that the magnetization pattern near the tag center is complex and difficult to predict. In practice, the center of the radial tag pattern is placed in the LV blood pool and subsequent convection mixes the blood signal and eliminates any tag pattern inside the LV cavity. In the CRT images, the LV blood pool tag signal is further reduced by image subtraction, which produces dark blood LV images while the radial tagging pattern remains apparent in the myocardial wall throughout the cardiac cycle.

As described in Eq. 1, RT images contain both tag and image information while CRT images contain only enhanced tag contrast information. With the additional use of the RFA scheme, the CRT tag contrast remains relatively constant throughout the entire cardiac cycle.

CRT also suppresses background tissues outside the heart as a consequence of image subtraction and the shallow tagging pattern, which fades quickly. This contrast property is being further explored as a means for enabling segmentation of the heart for quantitative evaluation of LV function.

Both RT and CRT tag profiles are affected by the RF pulse duration, tag number, amplitude of the RF pulse, and gradients lobes. In this article, these parameters were particularly chosen to make sure spins at the LV myocardial radius have the highest tag contrast, whereas the contrast for other tissues still follows the approximation in Eqs. 4 and 5. The relationship of the tag profile

as a function of the above parameters needs to be further studied.

The center of the radial tags should be at the center of the LV cavity to obtain the best radial tagging pattern. This can be achieved by moving the table to an optimal position. However, image quality decreases dramatically if the images are acquired outside of the gradient linearity range. A retrospective analysis of the clinical data shows that our sequence can generate acceptable tag pattern quality for a majority of patients (over 99%). Even with observable tag pattern imperfections, CRT may still provide useful landmarks for the assessment of cardiac function.

CRT images can be generated from the subtraction of the two sets of radial tagging images in several ways. We initially used an inversion pulse after the radial tags and subtracted the two sets to generate CRT images. However, this resulted in a blurry tag edge profile due to the asymmetric pattern of the inverted and noninverted magnetization. Our current method using a phase shift between the two sets of tag profiles, conversely, produces shaper tag profiles and results in better quality CRT images.

CRT images require the subtraction of the two sets of radial tagged images, which are acquired in a single breath hold. Our current sequence scheme acquires the first set of images completely before acquiring the second set of images. Therefore, high image quality depends on the subject's breath hold stability. A small movement of the diaphragm during the breath hold can result in poor tag and image quality after image subtraction. This may be improved by interleaving the two sets of radial tagging acquisitions to further minimize the potential subtraction error. Currently, the acquisition duration for the CRT sequence is ~ 20 s. While it is not a difficult task for a healthy adult, this can be challenging for patients and children with impaired cardiac or respiratory function.

The CRT method generates a tag pattern with enhanced tag contrast that better matches the annular shaped LV myocardial wall in SA images. These properties may enable more accurate measurements of the LV rotational mechanics, including LV twist and torsion or measures like circumferential strain, especially in mid-diastasis and late diastolic cardiac phases. Currently, the Fourier analysis of stimulated echoes analysis method is validated for line tagged images to provide a global LV twist measurements, but needs to be further evaluated for application to CRT patterns. A previous study also indicates that the RT technique can estimate regional LV rotation (19) and an extension to CRT should be evaluated. Future work involves developing a faster and robust analysis method, then evaluating accuracy, precision, and reproducibility in a clinical setting.

CONCLUSIONS

In conclusion, the CRT technique is a novel myocardial tagging method that generates high tag contrast in the later cardiac phases. It can be potentially used for

evaluating cardiac function and performing quantitative analysis of LV rotational function.

REFERENCES

1. Zerhouni EA, Parish DM, Rogers WJ, Yang A, Shapiro EP. Human heart: tagging with MR imaging–a method for noninvasive assessment of myocardial motion. Radiology 1988;169:59–63.
2. Axel L, Dougherty L. MR imaging of motion with spatial modulation of magnetization. Radiology 1989;171:841–845.
3. Ennis DB, Epstein FH, Kellman P, Fananapazir L, McVeigh ER, Arai AE. Assessment of regional systolic and diastolic dysfunction in familial hypertrophic cardiomyopathy using MR tagging. Magn Reson Med 2003;50:638–642.
4. Herzka DA, Guttman MA, McVeigh ER. Myocardial tagging with SSFP. Magn Reson Med 2003;49:329–340.
5. Fischer SE, McKinnon GC, Maier SE, Boesiger P. Improved myocardial tagging contrast. Magn Reson Med 1993;30:191–200.
6. Nasiraei-Moghaddam A, Finn JP. Tagging of cardiac magnetic resonance images in the polar coordinate system: physical principles and practical implementation. Magn Reson Med 2014;71:1750–1759.
7. Fonseca CG, Backhaus M, Bluemke DA, et al. The Cardiac Atlas Project–an imaging database for computational modeling and statistical atlases of the heart. Bioinformatics 2011;27:2288–2295.
8. Kellman P, Arai AE, Xue H. T1 and extracellular volume mapping in the heart: estimation of error maps and the influence of noise on precision. J Cardiovasc Magn Reson 2013;15:56.
9. Walker PM, Marie PY, Mezeray C, Bessieres M, Escanye JM, Karcher G, Danchin N, Mattei S, Villemot JP, Bertrand A. Synchronized inversion recovery-spin echo sequences for precise in vivo T1 measurement of human myocardium: a pilot study on 22 healthy subjects. Magn Reson Med 1993;29:637–641.
10. Di Donato M, Dabic P, Castelvecchio S, et al. Left ventricular geometry in normal and post-anterior myocardial infarction patients: sphericity index and 'new' conicity index comparisons. Eur J Cardiothorac Surg 2006;29(Suppl 1):S225–S230.
11. Stuber M, Spiegel MA, Fischer SE, Scheidegger MB, Danias PG, Pedersen EM, Boesiger P. Single breath-hold slice-following CSPAMM myocardial tagging. Magma 1999;9:85–91.
12. Griswold MA, Jakob PM, Heidemann RM, Nittka M, Jellus V, Wang J, Kiefer B, Haase A. Generalized autocalibrating partially parallel acquisitions (GRAPPA). Magn Reson Med 2002;47:1202–1210.
13. Reyhan M, Natsuaki Y, Ennis DB. Off-resonance insensitive complementary spatial modulation of magnetization (ORI-CSPAMM) for quantification of left ventricular twist. J Magn Reson Imaging 2014;39:339–345.
14. Reyhan M, Natsuaki Y, Ennis DB. Fourier analysis of STimulated echoes (FAST) for the quantitative analysis of left ventricular twist. J Magn Reson Imaging 2012;35:587–593.
15. Sengupta PP, Tajik AJ, Chandrasekaran K, Khandheria BK. Twist mechanics of the left ventricle: principles and application. JACC Cardiovasc Imaging 2008;1:366–376.
16. Herzka DA, Guttman MA, McVeigh ER. Myocardial tagging with SSFP. Magn Reson Med 2003;49:329–340.
17. Dietrich O, Raya JG, Reeder SB, Reiser MF, Schoenberg SO. Measurement of signal-to-noise ratios in MR images: influence of multichannel coils, parallel imaging, and reconstruction filters. J Magn Reson Imaging 2007;26:375–385.
18. Jovicich J, Czanner S, Greve D, et al. Reliability in multi-site structural MRI studies: effects of gradient nonlinearity correction on phantom and human data. NeuroImage 2006;30:436–443.
19. Kaveh R, Moghaddam AN, Khan SN, Paul JF. Regional rotation of the left ventricle in healthy and cardiomyopathic subjects measured with radial myocardial tagging. J Cardiovasc Magn Reson 2014;16(Suppl 1):P24.